Paleomagnetism of the Carboniferous–Permian Myall blocks, Tamworth Belt, southern New England Orogen: Permian counterclockwise rotations and Triassic clockwise rotation

C. Klootwijk
Research School of Earth Sciences, The Australian National University, Canberra, ACT 2601, Australia

*CONTACT Chris Klootwijk email*chris.klootwijk@anu.edu.au

Received 31 March 2021; accepted 22 September 2021
Editorial handling: Chris Fergusson

SUPPLEMENTAL DATA

Australian Journal of Earth Sciences (2022), 69, https://doi.org/10.1080/08120099.2022.1989033

Copies of Supplementary Papers may be obtained from the Geological Society of Australia's website (www.gsa.org.au), the Australian Journal of Earth Sciences website (www.ajes.com.au) or from the National Library of Australia's Pandora archive (https://pandora.nla.gov.au/tep/150555).

Supplemental data

Sampling detail
Magnetisation components
Rock magnetic results
Supplemental references

Sampling detail

western Myall Block

Wootton beds

Upper Tournaisian to middle Visean Wootton beds from the southern Girvan Anticline have been sampled in shallow-dipping siliceous mudstones/tuffaceous siltstones (sites 1–3, Figures 1 and 2, Table S1) interbedded with coarse-grained lithic sandstones (Buck, 1988; Roberts *et al.,* 1991). The sites are thought positioned higher up in the stratigraphically extended Wootton beds succession for dominance of mudstones and location near the overlying CongerFormation and Nerong Volcanics.

Conger Formation

Sampled in massive fine-to-medium grained sandstones (sites 4, 5) in a fault-duplicated section to the west of the Gloucester Syncline. The uppermost Conger Formation contains several rhyodacitic/andesitic ignimbrites and transitions into the Nerong Volcanics of middle to late Visean age (Roberts *et al*., 1991).

Nerong Volcanics – forearc basin

Nerong Volcanics occur widely throughout the western Myall Block, both in the forearc basin and in the arc complex at Port Stephens (Buck, 1988; Crane & Hunt, 1979; Roberts *et al*., 1991). They were previously correlated with the Martins Creek Ignimbrite Member (MCIM) of the Gresford and Rouchel blocks (Roberts *et al*., 1991). Dating of the Nerong Volcanics at 338.6 ± 1.8 Ma and the MCIM at 332.3 ± 2.2 Ma (Roberts *et al*., 1995a, 1995b, SL13 ages) instead favoured correlation of the Nerong Volcanics with the upper Isismurra Formation (unnamed ignimbrites near Albano, and north and east of Albano, members) of the Rouchel Block (Glen & Roberts, 2012) (Figure 2). The Nerong Volcanics are also correlated with the Buggs Creek Volcanic Member of the basal Berrico Creek Formation which outcrops northwest of the Gloucester Syncline and was studied paleomagnetically by Geeve (2000) and Geeve *et al.* (2002) (Figure 1). An extended series of massive Nerong Volcanics of grey- to purple-bluish, in part lithic, hematitic, mainly rhyodacitic ignimbrites (sites 9–15) has been sampled along the Nerong Forestry Road on the eastern limb of the Girvan Anticline (Crane & Hunt, 1979). Three sites (6–8) of similar volcanics sampled at the western base of the forestry road section may be transitional with the Conger Formation. Another four sites (17–20) of pinkish-purple and brownish-purple rhyodacitic ignimbrites have been sampled at two locations at Conger Hill on the western limb of the Girvan Anticline. A single site (16) of massive, fine-to- medium grained sandstone has been sampled on the western limb of the Gloucester Syncline.

Nerong Volcanics – arc complex

A further fifteen sites (21–35) have been sampled in Nerong Volcanics from the arc complex at Port Stephens (Buck, 1988). The exposed succession is made up of the areally limited, faulted and moderately-steep dipping, Fly Point rhyolitic ignimbrite, the overlying and likewise dipping Nelson Bay dacitic ignimbrite (21–24) and the in turn overlying, more widespread, Port Stephens rhyolitic ignimbrite (25–35) with mainly regional shallow SSW to WSW dips. The Fly Point and Nelson Bay ignimbrites are of laminated appearance for their strong alignment of flattened pumice clasts, whereas the Port Stephens ignimbrite is generally of massive appearance with occasional columnar jointing. Buck (1988) correlated the Port Stephens rhyolitic ignimbrite and the Nelson Bay dacitic ignimbrite with rhyodacitic ignimbrites and an andesitic ignimbrite at the Nerong Forestry Road section. He also identified a prominent gravity anomaly some 5 km to the southeast of Morna Point (Figure 1, MP) as the inferred source of the proximal ignimbrites, based on flow-lineation and movement sense in the Nelson Bay and Port Stephens ignimbrites. A sample from the latter (Morna Point, also sites 30, 31) has been dated at 340.5 ± 2.0 Ma (Chisholm *et al*., 2014, TEMORA 2/OG1 age). The Port Stephens region is dissected by several NNE–SSW faults that postdate regional folding (Buck, 1988) and align with the major Tarean Fault to the west. The region is further dissected by WNW–ESE faults with various southward repeats of the Nerong Volcanics succession. The Port Stephens region is heavily dissected by doleritic dykes that strike parallel to the two sets of faults and may be related to opening of the Tasman Sea (Buck, 1988).

Raymond Terrace dacite

The overlying Berrico Creek and Faulkland formations have not been sampled for limited occurrence (Berrico Creek), or absence (Faulkland), of suitable volcanics. However, four sites (36–39) of a dacitic flow of Faulkland Formation-equivalent age have been sampled in a quarry at Raymond Terrace, just east of the Williams River Fault (Figure 1) – three sites in columnar jointed blue-grey hematitic, lithic, ignimbrite in the quarry wall (37–39) and one site in the quarry floor (36) in large blocks that proved not in-situ. The dacite was originally mapped as the very top of the Italia Road Formation and was thought correlatable with the Paterson Volcanics (Rattigan, 1966), dated at 328 ± 1.4 Ma (Claoué-Long *et al.*, 1995, SL13 age), but is likely located slightly higher up in the stratigraphy (Roberts *et al.*, 1991, citing D. Mason pers. comm.). The Italia Road Formation and underlying Balickera Conglomerate (Rattigan, 1966) have been correlated with the Johnstone Formation of the Gresford Block, though apparently not with the age-equivalent Faulkland Formation of the western Myall Block (Roberts *et al.*, 1991) (Figure 2).

Booral Formation and McInnes Formation

The in turn overlying Booral Formation passes gradually upward into the McInnes Formation. Both have been sampled across both limbs of the Gloucester Syncline in moderately-to-steeply dipping, occasionally overturned, beds – the Booral Formation in siliceous mudstone (40–46), an occasional tuff (44, in part) and fine-to-medium grained sandstone (47, 48), and the McInnes Formation in volcanogenic sandstone (49) and whitish rhyolite (50) (Figure 1). The Booral and McInnes formations contain brachiopods of the *Levipustula levis* Zone (Roberts *et al.*, 1991) and both have been assigned to the lowermost–upper Carboniferous Serpukhovian Stage (Glen & Roberts, 2012) (Figure 2).

Alum Mountain Volcanics

The conformably overlying Johnsons Creek Conglomerate, also of Serpukhovian age, has not been sampled for paucity of suitable volcanics. It is overlain disconformably and with a very substantial hiatus in age by the lower Permian Alum Mountain Volcanics. Fourteen sites (51–64) have been sampled in variegated rhyolites, often flow-banded and occasionally welded, on both, steeply-dipping to locally overturned, limbs of the Gloucester Syncline. A pollen assemblage indicating Stage 3a (Helby *et al.*, 1986; McMinn, 1987; Roberts *et al.*, 1991) dates the lower part of the Alum Mountain Volcanics succession as early Sakmarian (Cawood *et al.*, 2011a; Roberts *et al.*, 1991; Veevers, 2013; Young & Laurie, 1996), possibly late Asselian (Caprarelli & Leitch, 1998; Champion, 2016), and this is also taken as the formation age of the Gloucester Syncline. It is unfortunate that radiometric dates for an unspecified Alum Mountain Volcanic site at the Gloucester Syncline (Li *et al.*, 2014, 271.8 ± 1.8 Ma, $^{40}Ar/^{39}Ar$ age) and for the Lakes Road Rhyolite Member of the upper Alum Mountain Volcanics at the Myall Syncline (Roberts, Claoué-Long, Jones & Foster, 1995; Roberts *et al.*, 1996, 274.1 ± 3.4 Ma, SL13 age) have been taken as representative for the entire Alum Mountain Volcanics succession (Glen, 2005; Glen & Roberts, 2012; Shaanan *et al.*, 2015). This in spite of previous opinions, based on above-detailed well-established palynological evidence, for an extended development over time (Briggs, 1998; Roberts *et al.*, 1991, 1996; Roberts, Claoué-Long, Jones & Foster, 1995), ranging from Stage 3a to Upper Stage 4b, possibly Lower Stage 5a (McMinn, 1987) and equating in age from late Asselian/early Sakmarian to late Artinskian (Price, 1983; Young & Laurie, 1996).

Durallie Road Formation

A further two sites (65, 66) have been sampled in slightly-welded, moderately-dipping, pinkish-greyish to purplish-reddish tuffs of the Durallie Road Formation in the south central part of the Gloucester Syncline. The Durallie Road Formation seems to disconformably overlie the Alum Mountain Volcanics, is itself conformably overlain by coal horizons with a well-established Lower Stage 5a pollen flora (Helby *et al.*, 1986), and has been assigned accordingly to Upper Stage 4b – possibly Lower Stage 5a (McMinn, 1987). There is less clarity about the actual age of the Durallie Road Formation. It has been equated with the Ufimian by Roberts *et al.* (1991), would be equated with the late Artinskian following the Young & Laurie (1996) timescale, and has been assigned to the Kungurian (ca 272–266 Ma) by Briggs (1998). Recent CA-IDTIMS-based recalibration of Australian late Permian palynostratigraphy has resulted in younging the Upper Stage 5a by

some two million years and equating it with the Roadian/Wordian (Laurie *et al.*, 2016). This leaves an uncomfortably broad age for the Durallie Road Formation, ranging from a possible late Artinskian to a possible early Wordian age.

eastern Myall Block

Reconnaissance sampling has been confined to the southwestern part of the eastern Myall Block,in the Myall Syncline and eastward adjacent fault blocks (Figure 1), in three stratigraphic unitswith suitably developed tuffs and tuffaceous beds for comparison with western Myall Block counterparts (Figure 2).

Nerong Volcanics. Sampled in the eastern limb of the Myall Syncline across a NNW-trending,steeply west dipping, tectonised section of silicified tuffaceous silts (68, 69) and a bluish tuff (70) along the Pacific Highway (Crane & Hunt, 1979; Roberts *et al.,* 1991). A blue-grey tuff (67)has been sampled along the Great Lake Way in an eastward adjacent, moderately steep dipping,fault block succession (Figure 1).

Yagon Siltstone

Sampled at three locations in an eastward adjacent fault block across a stratigraphic succession correlatable with the Booral and McInness formations of the western Myall Block (Figures 1 and 2), along the Great Lakes Way in dark-blue tuffaceous siltstone (71), along the Old Pacific Highway at O'Sullivans Gap in well-banked dark-grey siliceous mudstone (72–74), and just south of O'Sullivans Gap in massive dark-grey siliceous mudstone of the Violet Hill Volcanic Member (75) (Crane & Hunt, 1979; Roberts *et al.*, 1991).

Alum Mountain Volcanics

Sampled in the steeply northeast dipping western limb of the Myall Syncline at Burdekins Gap along the Pacific Highway. Sampling has been confined to a well-exposed section of the Lakes Road Rhyolite Member in flow-banded purplish rhyolite (76–80) (Crane & Hunt, 1979; Jenkins & Nethery, 1992; Roberts *et al.*, 1991). The Lakes Road Rhyolite Member is the stratigraphically highest unit of the Alum Mountain Volcanics at the Myall Syncline (Jenkins & Nethery, 1992). Roberts *et al.* (1995b) interpret a pollen assemblage, recorded by J. P. F. Hennelly (1961, unpublished report) that may have come from the boundary between the Lakes Road Rhyolite and the underlying Burdekin Gap Basalt, as Stage 4, possibly Stage 3b. It is unfortunate that an about 274 Ma SL13 date for the Lakes Road Rhyolite (Roberts, Claoué–Long, Jones & Foster, 1995; Roberts *et al.*, 1996) and an about 272 Ma $^{40}Ar/^{39}Ar$ date from the Gloucester Syncline (Li *et al.*, 2014a) have been taken as representative for the entire Alum Mountain Volcanics succession across both synclines (Glen & Roberts, 2012; Shaanan *et al.*, 2015), in spite of palynological evidence for substantially older bases of the successions at the Gloucester and Myall synclines as acknowledged by Roberts, Claoué–Long, Jones & Foster (1995) and Roberts *et al.* (1996). The Alum Mountain Volcanics at the Myall Syncline have been heavily affected by low–to–moderate temperature (around 200°C) hydrothermal alterations (Jenkins & Nethery, 1992) which may have contributed to the observed pervasive remagnetisation of the Lakes Road Rhyolite Member.

Magnetisation components

This is a descriptive analysis of observed magnetisation components, exemplified from an extended overview of representative Zijderveld plots (Figure S4 a–bbb).

western Myall Block

Wootton beds

The three sites (1–3) (Figure S4 a, b) show a well-developed low-temperature component resembling the mid Cenozoic overprint observed throughout the other TB studies. One site (1) shows just a single high-temperature component (T) of ENE declination and very steep (+) inclination, indicating a late Permian–Early Triassic overprint of reverse polarity. The other two sites (2, 3) (Figure S4 a, b) show well-defined intermediate- (O) and high-temperature (P) components with opposing polarities between the two sites for each of the two components. Both components have NW or SE declinations and moderate (+ or –) inclinations. Comparison with the SNEO pole path suggests a mid Carboniferous overprint origin for the O

component and a primary late-early Carboniferous origin for the P component. A few samples of one site (3) (Figure S4 b) show a moderately steep (+) high-temperature component (T) suggesting a mid Triassic overprint.

Conger Formation

The sandstone sites (4, 5) (Figure S4 c, d) show a minor low-temperature (L) component and a well-developed high-temperature (T) component of ESE declination and steep (+) inclination suggesting a mid Triassic overprint. Thermal (Figure S4 d), and less so AF (Figure S4 c), demagnetisations at intermediate temperature/coercivity ranges show a consistent directional pattern that belies composite breakdown of the L and T components and indicates presence of two (O, TT) intermediate-temperature components. The WNW declination and low (+) inclination of the softer O component suggests a mid Carboniferous overprint origin whereas the western declination and moderately steep (+) inclination of the TT component suggests a latest Carboniferous–earliest Permian overprint.

Conger Formation/basal Nerong Volcanics

Tuffs near the transition (6–8) on the forestry road section on the eastern limb of the Girvan Anticline show a consistent pattern of well-developed low- (L) and high-temperature (P, O) components (Figure S4 e, f), with one site (7) showing persistent presence of an intermediate-temperature (O) component. The W declination and very low (–) inclination of the high-temperature component (P) for two of the sites (7, 8) suggests a primary origin. The high-temperature component (O) of site 6 agrees directionally with the intermediate-temperature component (O) of site 7 (Figure S4 e, f), with their W declination and low (+) inclination suggesting a mid Carboniferous overprint.

Nerong Volcanics – forearc basin

Upward succeeding tuffs (9–15) (Figure S4 g–i) from the forestry road section show a comparable, yet more complex, magnetisation pattern with well-developed low- (L) and high-temperature components (O, T), and also persistent presence of one (P: 9, 11) (Figure S4g), or two successive (P, O: 10, 12) (Figure S4 h), intermediate-temperature components. Their consistency, and the obvious directional interpretation of one of these two intermediate-temperature components as primary (P), supports their reality and all but rules out that they merely reflect composite breakdown of low- and high-temperature components. The intermediate-temperature P components in the stratigraphically lower Nerong Volcanics sites (9–12) are all of normal polarity and correspond directionally – western declinations and low- to- moderate (–) inclinations – with normal polarity, but high-temperature, P components in underlying tuffs of the Conger Formation/Nerong Volcanics transition beds (7, 8). They also correspond directionally with reverse polarity, ENE declinations and moderate (+) inclinations, high-temperature P components in stratigraphically higher Nerong Volcanics sites (14, 15). Notably, the Nerong Volcanics sites with intermediate-temperature normal polarity P components also show high-temperature components that either represent a reverse polarity mid Carboniferous overprint (O: site 13) with ENE declination and moderate (–) inclination, or late Permian–Early Triassic (T: 10) or mid Triassic (T: 11, 12) normal polarity overprints with very steep (–) or slightly less steep (–) inclinations. It seems that multiple pervasive overprintings of these MD volcanics may have left untouched a remainder primary magnetisation component in intermediate unblocking temperature ranges.

A sandstone bed from the Nerong Volcanics succession sampled close to a substantial fault on the southwestern limb of the Gloucester Syncline (Figure 1: 16), shows a well-defined L-component and a reasonably well-defined high-temperature component of reverse polarity with eastern declination and moderate to steep (+) inclination suggesting a mid Triassic overprint (Figure S4 j).

Two tuff sections sampled in stratigraphically lower (17, 18) and upper parts (19, 20) of the Nerong Volcanics on the western limb of the Girvan Anticline (Figure 2, Conger Hill) show complex magnetisations not unlike their Nerong Volcanics counterparts on the eastern limb (9– 15, Nerong Forestry Road section). The stratigraphically lower two sites (17, 18), weathered-out corestones, are unusual in showing no, or poorly developed, L-component directions (Figure S4 k) with northern declinations but with low to moderate (–) inclination that do not seem of mid Cenozoic origin and could be of lightning origin. Site 17 shows mainly a

high-temperature primary component of normal polarity with northwestern declination and low to moderate (–) inclination and an occasionally developed high coercivity reverse polarity component of northern declination and moderate to steep (+) inclination that suggests a mid Triassic overprint. Site 18 in contrast, shows an intermediate-temperature/low coercivity primary component of normal polarity western declination and low to moderate (–) inclination with a high-temperature/high coercivity reverse polarity component (Figure S4 k) of northern declination and moderate to steep (+) inclination likewise suggesting a mid Triassic overprint. The upper two sites (19, 20) show equally complex magnetisations with well-developed low-temperature components and high- temperature primary (P) and overprint (O) components that have counterparts in intermediate unblocking temperature ranges (Figure S4 l). The high-temperature primary component of reverse polarity with eastern declination and low (+) inclination is well developed in site 20 but not so in site 19, whereas the high-temperature overprint component of reverse polarity with eastern declination and moderate (–) inclination suggestive of a mid Carboniferous overprint is well developed in both sites.

Nerong Volcanics – arc complex

Volcanics from the Port Stephens arc complex show consistent demagnetisation behaviour across all sites (21–35) sampled from the two stratigraphically higher ignimbrites (Figure S4 m–w). However, sites (27–29) from the Diemars quarry in the northwest of the Port Stephens area (Figures 1 and S4 q–t) do show for all identified components, bar the low-temperature (L) component, declinations that deviate clockwise from counterparts for other Port Stephens sites, probably reflecting local tectonics of the Diemars quarry area.

Demagnetisation behaviour of the arc complex Nerong Volcanics is comparable to that of the forearc basin Nerong Volcanics. The arc volcanics show a generally well-developed low-temperature (L) component indicative of the customary mid Cenozoic overprint, a well-developed high-temperature (T) component of exclusively reverse polarity with moderate to steep (+) inclination and NW declination indicative of a latest Carboniferous–earliest Permian overprint (Figure S4 q, r, v, w), and also high-temperature (T, N) components of both normal and reverse polarity and steep to very steep (+, –) inclinations indicative of a mid Triassic overprint (Figure S4 n–p). A few sites (30, 32, 35) also show a very-low-temperature (Tn) component of NE declination and steep to very steep (–) inclination (Figure S4 v) that likewise seems a mid Triassic overprint. The Diemars quarry sites (27–29) show high-temperature components (T1, T2) of exclusively reverse polarity with steep (+) inclinations and northern declinations indicative of a mid Permian overprint and also a very-high-temperature component (T3) of very steep (+) inclination indicative of a late Permian–Early Triassic overprint (Figure S4 s, t). A single site from the Morna Point area (Figure 1: 31) shows a high-temperature (O) component of normal polarity with low to moderate (+) inclination and WNW declination indicative for a mid Carboniferous overprint (Figure S4 u), comparable to intermediate-temperature (O) components in other arc volcanics sites. The arc volcanics also show, like the forearc basin Nerong Volcanics, less well-developed but directionally consistent intermediate-temperature components of exclusively normal polarity with low (–) inclination and NW (P) or northern (N, Diemars quarry) declinations indicative of a primary origin, often in combination with a slightly harder intermediate-temperature component with low to moderate (+) inclination and WNW (O) or NWN (Q, Diemars quarry) declinations indicative of a mid Carboniferous overprint (Figure S4 n, o, q–v).

Raymond Terrace dacite

One site (36) sampled in the quarry base shows directional results that are incongruent between the individual blocks sampled, which apparently were not in-situ. The other three sites (37–39) sampled across the quarry wall show a consistent pattern of a low-temperature (L) component of mid Cenozoic origin and a high-temperature (P) component with steep to very steep (+) inclination and S declination indicative of a primary origin (Figure S4 x, y). Sites 38 and 39 also show occasional presence of high-temperature (S, Q) components of normal polarity, steep (–) inclination and N declination indicating a mid Triassic overprint (Figure S4 y).

Booral Formation

Mudstone and sandstone sites (40–48) mostly show a consistent pattern of a low-temperature (L) component of mid Cenozoic origin and an intermediate- to high- temperature component (T) of exclusively reverse polarity with steep (+) inclination and with S or E declination indicating a latest Carboniferous–earliest Permian or a mid Triassic overprint respectively, or with very steep (+) inclination indicating a late Permian–Early Triassic (T) overprint (Figure S4 cc–ff). Two sites (40, 43) show also an intermediate-temperature (40) or an intermediate-to high-temperature (43) component, both of reverse polarity, with moderate (+) inclination and western declination indicative of a latest Carboniferous–earliest Permian (O) overprint (Figure S4 aa, bb).

McInnes Formation.

Two sites (49, 50) consistently show the customary low-temperature (L) component, albeit with very steep (–) inclinations for site 49, and a high-temperature component of reverse polarity with either very steep (+) inclination indicating a late Permian–Early Triassic (T, 49) overprint or steep (+) inclinations indicating a mid Permian overprint (T, 50) (Figure S4 gg, hh). The latter site also shows a minor intermediate-temperature (Tn) component as a normal polarity conjugate to the reverse polarity high-temperature (T) component (Figure S4 hh).

Alum Mountain Volcanics

Part of the sites at the Gloucester Syncline (51–64) show a well-developed low-temperature (L) component and a reverse polarity high-temperature component (P) of moderate to steep (+) inclination, with the SW declinations of the stratigraphically higher sites (59, 60, 63, 64) (Figure S4 nn, oo) indicating a primary origin and with the clockwise-deflected SSE declinations of the stratigraphically lower sites (52, 54, 55) (Figure S4 ii, jj) probably indicative of an intra-formational tectonic disturbance. High-temperature components for the other sites show either both reverse and normal polarities and very steep (+, –) inclinations and NW declinations indicating a late Permian–Early Triassic overprint (51, 61), or both reverse and normal polarities and steep to very steep (+, –) inclinations and W or E declinations indicating a mid Triassic overprint (53, 56, 57, 58, 62) (Figure S4 kk, ll). Several sites (56, 58, 62) show an additional component, being either a reverse polarity post-folding component (Lr) in the intermediate temperature range (Figure S4 mm, 62), or a normal polarity post-folding component (Lh) in the high temperature range (Figure S4 ll, 58), or a high-temperature component (Q) (Figure S4 kk, 56) with poorly-grouped directions and of unclear origin, probably attributable to the soft, permeable, constitution of the Gloucester Buckets rhyolite.

Durallie Road Formation

Two sites (65, 66) show a simple pattern of a minor low-temperature (L) component and very well-developed high-temperature P subcomponents across magnetite (P0, P1) and hematite (P2) unblocking temperature ranges (Figure S4 pp). The WSW declination and steep (+) inclination of the reverse polarity P2 subcomponent indicates a late-early to mid Permian primary magnetisation offset counterclockwise with respect to the Permian KG pole path. The formation is the youngest stratigraphic unit of the Myall blocks studied herein and carries importance in defining the youngest time limit on rotation based on a primary magnetisation result.

eastern Myall Block

Nerong Volcanics

Tuffaceous beds (68, 69) and tuffs (70, 67) from the forearc basin of the eastern Myall Block show comparable magnetic behaviour to the Nerong Volcanics from both forearc basin and arc in the western Myall Block (Figure S4 qq–uu). Sites 68 to 70 and part of site 67 show consistent presence of a substantial low-temperature (L) component of mid Cenozoic origin, an intermediate-temperature component of mainly reverse polarity with moderate (+) inclination and NE declination indicating a primary component (P) offset substantially counterclockwise compared with the SNEO pole path, and a high-temperature component (T) of reverse polarity with very steep (+) inclination indicating a late Permian–Early Triassic overprint (Figure S4

qq–ss). One of the tuffs (67) shows for part of its sampled section a substantial high-temperature primary component (Pn) of SSW declination and moderate (–) inclination (Figure S4 uu) representing a normal polarity conjugate to the predominant reverse polarity intermediate-temperature component in the remainder of the site (Pr) (Figure S4 tt) and in the other Nerong Volcanics sites (P) (Figure S4 qq–ss). Several samples from site 67 also show a minor intermediate-temperature component of very steep (–) inclination (Tn) as a normal polarity conjugate to the predominant reverse polarity high-temperature (T) late Permian–Early Triassic overprint (Figure S4 tt).

Yagon Siltstone

Tuffaceous siltstone (71) and siliceous mudstone sites (72–75) show a well-developed low-temperature (L) component and a high-temperature (T) component of reverse polarity and very steep (+) inclination indicating a late Permian–Early Triassic overprint (Figure S4 vv–zz). Two sites (73, 75) show no composite breakdown whatsoever of the L and T components (Figure S4 xx, zz). The single site (75) of the Violet Hill Volcanic Member of the Yagon Siltstone also shows a rather poorly developed intermediate-temperature component (P) of reverse polarity with NE declination and moderate (+) inclination indicating a primary magnetisation offset substantially counterclockwise compared with the SNEO pole path (Figure S4 zz).

Alum Mountain Volcanics

Purplish rhyolite sites (76–80) of the Lakes Road Rhyolite Member show a consistent pattern of dual polarity low-temperature components (Ln, Lr) and dual polarity high-temperature components (T, PT) (Figure S4 aaa, bbb). The softer normal polarity low-temperature component (Ln) represents the omnipresent mid Cenozoic overprint. The less widely present harder reverse polarity low-temperature component (Lr) (Figure S4 aaa) shows a lower inclination, indicative of a more recent overprint origin during the Cenozoic steady northward movement of Australia. The dominant high-temperature component (T) of reverse polarity, eastern declination and steep to very steep (+) inclination indicates a mid Triassic overprint (Figure S4 aaa, bbb). The less widely present, minor, very high-temperature component (PT) of normal polarity, SW declination and steep (–) (76, 77) or very steep (–) inclinations (78) indicates likewise a mid Triassic overprint (Figure S4 aaa).

Rock magnetic results

IRM acquisition and three-axis Lowrie test

IRM acquisition curves (Figure S5 a–l) show for most stratigraphic units magnetite saturation at 200–700 mT (Figure S5 a–c, e, f, j–l), with the McInnes and Duralie Road formations showing lack of hematite saturation at 2.7 T (Figure S5 g, i). Nerong Volcanics of the Port Stephens arc complex and Alum Mountain Volcanics of the Gloucester Syncline show variety in behaviour from magnetite saturation at 200 mT to absence of hematite saturation at 2.7 T (Figure S5 d, h). Lowrie (1990) tests (Figure S5 m–ff) show presence throughout the stratigraphy of a low-coercivity component with unblocking temperatures generally in the magnetite range (540–580°C) (Figure S5 m–o, q, s, u–x, bb, dd, ee) but with notable exceptions of some Nerong Volcanics and some Alum Mountain Volcanics sites above 600°C (Figure S5 p, t, z), other Alum Mountain Volcanics sites around 400°C (Figure S5 aa), and the Lakes Road Rhyolite Member at 200–400°C (Figure S5 ff). Most stratigraphic units also show subordinate presence of a high- coercivity component in the hematite unblocking temperature range (600–690°C) (Figure S5 m–q, s–w, z–ff) or slightly lower unblocking temperatures for the McInnes Formation and some Alum Mountain Volcanics sites (Figure S5 x, y), but with more substantial presence in some Nerong Volcanics and Alum Mountain Volcanics sites (Figure S5 s, z) and with predominant presence in other Nerong Volcanics sites and in the Duralie Road Formation (Figure S5 r, cc).

Susceptibility cycling

Low-temperature cycling (Figure S6 a–l) shows for about half the stratigraphic units and notably the Nerong Volcanics, a susceptibility peak in the –160 to –150°C range indicative for the Verwey transition in MD and pseudo-single-domain (PSD) magnetite (Figure S6 b–e, h, j, k) (Kosterov, 2003; Muxworthy, 1999). High-

temperature cycling (Figure S6 m–ff) shows dominant presence of a magnetite phase with unblocking temperatures in the 550 to 600°C range (Figure S6 m–t, v–aa, dd, ee) and a hematite phase unblocking in the 600 to 700°C range (Figure S6 m–ff). High-temperature cycling also shows hump structures in the 100 to 500°C range of the heating curves indicative for maghemite-to-hematite conversion (Figure S6 n–p, r, s, u, v, y, z, bb, ff) with often consequently reduced susceptibility in the cooling curves (Figure S6 o–v, z, ff), whereas other cooling curves show substantially increased susceptibility indicative for magnetite formation (Figure S6 m, w–y, aa, dd, ee). These observations point to limited effectiveness of the low-level argon gas environment maintained over the heating-cooling cycle to prevent such phase changes. High-temperature cycling also shows Hopkinson peaks at 500 to 600°C in the heating curves (Figure S6 m–q, s, y, z, bb, dd, ee) indicative for single-domain (SD) magnetite (Clark & Schmidt, 1982; Dunlop & Özdemir, 1997).

Day plot, hysteresis loops and FORC diagrams

The Day plot (Figure S7) (Day *et al.*, 1977) shows the magnetisation of most sites residing in the PSD domain, with part of the Raymond Terrace dacite/Italia Road Formation sites residing in the MD domain. Alum Mountain Volcanics sites in particular show large variability in Bcr/Bc and Mr/Ms values. Most Nerong Volcanics sites from both arc and forearc basin do group in the PSD domain, with a sizable fraction verging into higher Bcr/Bc values and with two outliers showing very low or very high Bcr/Bc values.

Most hysteresis loops (Figure S8 a–p, upper figures) show closure well above 0.2–0.3 T (Figure S8 a–f, i, j, l, m, o, p) indicating widespread presence of a hematite carrier in addition to magnetite (Roberts *et al.*, 1995). Most hysteresis loops are pot-belly type, but the Durallie Road Formation loop is wasp-waisted (Figure S8 m) (Roberts *et al.*, 1995; Tauxe *et al.*, 1996), commensurate with IRM indication (Figure S5 i) for a substantial hematite presence. In contrast to the Day plot and as expected (Roberts *et al.*, 2018), the FORC diagrams (Figure S8 a–p, lower figures) are more informative on domain state, although mainly for the magnetite carrier which tends to swamp the hematite signature. FORC diagrams for sites from forearc basin Nerong Volcanics of both western and eastern Myall blocks, arc Nerong Volcanics from the Port Stephens region, the Raymond Terrace dacite/Italia Road Formation and the Lakes Road Rhyolite Member of the Alum Mountain Volcanics show contours diverging near the Bu-axis and asymmetric around Bu= 0 (Figure S8 c, d, g, n, p) characteristic for MD magnetite (Muxworthy & Roberts, 2007; Roberts *et al.*, 2000, 2006, 2014). Diagrams for the Conger Formation/Nerong Volcanics transition beds, most of the arc Nerong Volcanics, some of the Alum Mountain Volcanics and the Yagon Siltstone show contours with closure near the Bu-axis and vertical spread at low-to-moderate Bc values (Figure S8 b, e, f, j, l, o) indicative for PSD and/or MD domains with stronger domain wall pinning and/or possible interacting SD behaviour, with high Bc values for the Yagon Siltstone (Figure S8 o) indicating a hematite carrier. FORCdiagrams for the Wootton beds, the Durallie Road Formation and some of the forearc basin Nerong Volcanics sites from the eastern Myall Block uniquely show central ridge contours (Figure S8 a, m, n) indicative for non-interacting SD behaviour. A few diagrams of poor resolution from the McInnes Formation and the Alum Mountain Volcanics of the Gloucester Buckets suggest MD behaviour (Figure S8 i, k).

Supplemental references

Abdullah, R., & Rosenbaum, G. (2018). Devonian crustal stretching in the northern Tasmanides (Australia) and implications for oroclinal bending. *Journal of Geophysical Research, 123*, 7108–7125. https://doi.org/10.1029/2018JB015724

Briggs, D. J. C. (1998). Permian Productidina and Strophalosiidina from the Sydney-Bowen Basin and New England Orogen: systematics and biostratigraphic significance. *Association of Australasian Palaeontologists Memoir, 19.* 258 pp.

Caprarelli, G., & Leitch, E. C. (1998). Magmatic changes during the stabilisation of a cordilleran fold belt: the Late Carboniferous–Triassic igneous history of eastern New South Wales, Australia. *Lithos, 45*, 413–430.

Cayley, R., & Musgrave, R. (2015). The Giant Lachlan Orocline – a powerful new predictive tool for mineral exploration under cover across eastern Australia. In P. C. Lewis (Compiler), *Mineral exploration in the Tasmanides* (pp. 29–38). Australian Institute of Geoscientists Bulletin, 62.

Clark, D. A., & Schmidt, P. W. (1982). Theoretical analysis of thermomagnetic properties, low- temperature hysteresis and domain structure of titanomagnetites. *Physics of the Earth and Planetary Interiors, 30,* 300–316. https://doi.org/10.1016/0031-9201(82)90029-2

Crane, D. T., & Hunt, J. W. (1979). The Carboniferous sequence in the Gloucester-Myall Lake area, New South Wales. *Australian Journal of Earth Sciences, 26*(7–8), 341–352. https://doi.org/10.1080/00167617908729101

Day, R., Fuller, M., & Schmidt, V. A. (1977). Hysteresis properties of titanomagnetites: grain-size and compositional

dependence. *Physics of the Earth and Planetary Interiors, 13*, 260–267. https://doi.org/10.1016/0031-9201(77)90108-X

Doublier, M., Purdy, D. J., Hegarty, R. A., Nicoll, M. G., & Zwingmann, H. (2018). Structural elements of the southern Thomson Orogen (Australian Tasmanides): a tale of megafolds. *Australian Journal of Earth Sciences, 65*, 917–941. https://doi.org/10.1080/08120099.2018.1526213

Dunlop, D. J., & Özdemir, Ö. (1997). *Rock magnetism fundamentals and frontiers*. Cambridge University Press, 573 pp.

Fisher, R. A. (1953). Dispersion on a sphere. *Proceedings of the Royal Society of London, A217*, 295–305. https://doi.org/10.1098/rspa.1953.0064

Glen, R. A. (2005). *The Tasmanides of eastern Australia*. Geological Society, London, Special Publications, 246, 23–96. https://doi.org/10.1144/GSL.SP.2005.246.01.02

Helby, R., Lennox, M., & Roberts, J. (1986). The age of the Permian sequence in the Stroud-Gloucester Trough. *Journal and Proceedings, Royal Society of New South Wales, 119*, 33–42.

Jelinek, V. (1978). Statistical processing of anisotropy of magnetic susceptibility measured on a group of specimens. *Studia Geophysica et Geodaetica, 22*, 50–62. https://doi.org/10.1007/BF01613632

Jelinek, V. (1981). Characterization of the magnetic fabric of rocks. *Tectonophysics, 79*, 63–67. https://doi.org/10.1016/0040-1951(81)90110-4

Kosterov, A. (2003). Low-temperature magnetization and AC susceptibility of magnetite: effect of thermomagnetic history. *Geophysical Journal International, 154*, 58–71. https://doi.org/10.1046/j.1365-246X.2003.01938.x

Laurie, J. R., Bodorkos, S., Nicoll, R. S., Crowley, J. L., Mantle, D. J., Mory, A. J., Wood, G. R., Backhouse, J., Holmes, E. K., Smith, T. E., & Champion, D. C. (2016). Calibrating the middle and late Permian palynostratigraphy of Australia to the geological time-scale via U–Pb zircon CA-IDTIMS dating. *Australian Journal of Earth Sciences, 63(*6), 701–730. https://doi.org/10.1080/08120099.2016.1233456

McFadden, P. L. (1990). A new fold test for palaeomagnetic studies. *Geophysical Journal International, 103*, 163–169. https://doi.org/10.1111/j.1365-246X.1990.tb01761.x

McFadden, P. L., & McElhinny, M. W. (1990). Classification of the reversal test in palaeomagnetism. *Geophysical Journal International, 103,* 725–729. https://doi.org/10.1111/j.1365-246X.1990.tb05683.x

McMinn, A. (1987). Palynostratigraphy of the Stroud-Gloucester Trough, N.S.W. *Alcheringa, 11*(2), 151–164. https://doi.org/10.1080/03115518708618986

McPhie, J. (1987). Andean analogues for Late Carboniferous volcanic arc and arc flank environments of the western New England Orogen, New South Wales, Australia. *Tectonophysics, 138,* 269–288. https://doi.org/10.1016/0040-1951(87)90044-8

Muxworthy, A. R. (1999). Low-temperature susceptibility and hysteresis of magnetite. *Earth and Planetary Science Letters, 169*, 51–58. https://doi.org/10.1016/S0012-821X(99)00067-9

Muxworthy, A. R., & Roberts, A. P. (2007). First-order reversal curve (FORC) diagrams. In D. Gubbins & E. Herrero-Bervera (Eds.), *Encyclopedia of Geomagnetism and Paleomagnetism* (pp. 266–272). Springer.

Nakamura, A., & Milligan, P. R. (2015*). Total Magnetic Intensity (TMI) Image of Australia with Variable Reduction to Pole (VRTP), 1:5,000,000 scale*. http://www.ga.gov.au/ metadata-gateway/metadata/record/82800/

Phillips, G., Colquhoun, G. G., Hughes, K. S., & Deyssing, L. (2015). Seamless geology of New South Wales: approach, methodology and application. *Quarterly Notes Geological Survey of New South Wales, 145*, 1–25.

Price, P. L. (1983). A Permian palynostratigraphy for Queensland. In C. B. Foster (Ed.), *Permian Geology of Queensland* (pp. 155–211). Geological Society of Australia, Queensland Division.

Raymond, O. L., (Ed.) Gallagher, R., & Highet, L. M. (2012). *Surface geology of Australia, 1:2,500,000 scale, 2012 edition (Digital Dataset*). Geoscience Australia. http://www.ga.gov.au/metadata-gateway/metadata/record/73140/

Roberts, A. P., Cui, Y., & Verosub, K. L. (1995). Wasp-waisted hysteresis loops: mineral magnetite characteristics and discrimination of components in mixed magnetic systems. *Journal of Geophysical Research, 100*, 17909–17924. https://doi.org/10.1029/95JB00672

Roberts, A. P., Pike, C. R., & Verosub, K. L. (2000). First-order reversal curve diagrams: a new tool for characterizing the magnetic properties of natural samples. *Journal of Geophysical Research, 105*, 28461–28475. https://doi.org/10.1029/2000JB900326

Roberts, A. P., Liu Q., Rowan, C. J., Chang, L., Carvallo, C., Torrent, J., Horng, C.-S. (2006). Characterization of hematite (á-Fe2O3), goethite (á-FeOOH), greigite (Fe3S4), and pyrrhotite (Fe7S8) using first-order reversal curve diagrams. *Journal of Geophysical Research, 111*, B12S35, https://doi.org/10.1029/2006JB004715

Roberts, A. P., Heslop, D., Zhao, X., & Pike, C. R. (2014). Understanding fine magnetic particle systems through use of first-order reversal curve diagrams. *Reviews of Geophysics, 52*. https://doi.org/10.1002/2014RG000462

Roberts, A. P., Tauxe, L., Heslop, D., Zhao, X., & Jiang, Z. (2018). A critical appraisal of the "Day" diagram. *Journal of Geophysical Research, 123*, 2618–2644. https://doi.org/10.1002/2017JB015247

Shaanan, U., & Rosenbaum, G. (2018). Detrital zircons as palaeodrainage indicators: insights into southeastern Gondwana from Permian basins in eastern Australia. *Basin Research, 30*, Suppl. 1, 36–47. https://doi.org/10.1111/bre.12204

Tauxe, L., Mullender, T. A. T., & Pick, T. (1996). Potbellies, wasp-waists, and superparamagnetism in magnetic hysteresis. Journal of Geophysical Research, 101, 571–583. https://doi.org/10.1029/95JB03041

Young, G. C., & Laurie, J. R. (1996). *An Australian Phanerozoic Timescale*. Oxford University Press, 279 pp.

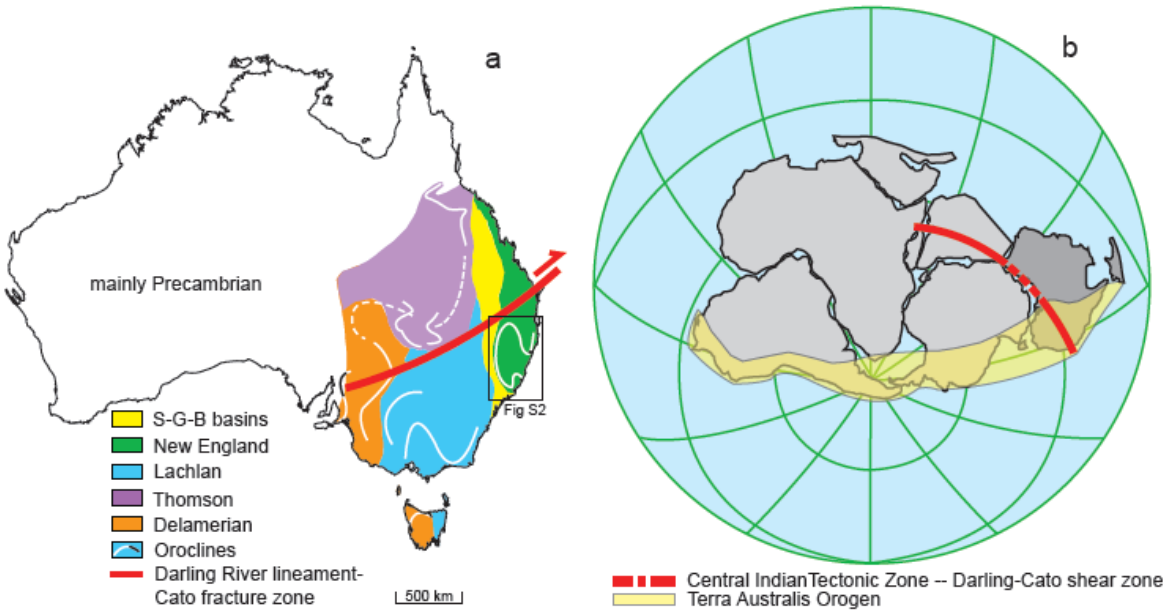

Figure S1. (a) Oroclinal structures in the Tasmanides after Abdullah and Rosenbaum (2018), Cayley and Musgrave (2015), Doublier et al. (2018), Glen (2013), Musgrave (2015), Phillips et al. (2016) and Rosenbaum (2018). S-G-B basins, Sydney-Gunnedah-Bowen basin system. (b) Gondwana reconstruction after Lawver and Scotese (1987) with Terra Australis Orogen after Cawood (2005). Central Indian Tectonic Zone-Darling River lineament-Cato fracture zone after Klootwijk (2013).

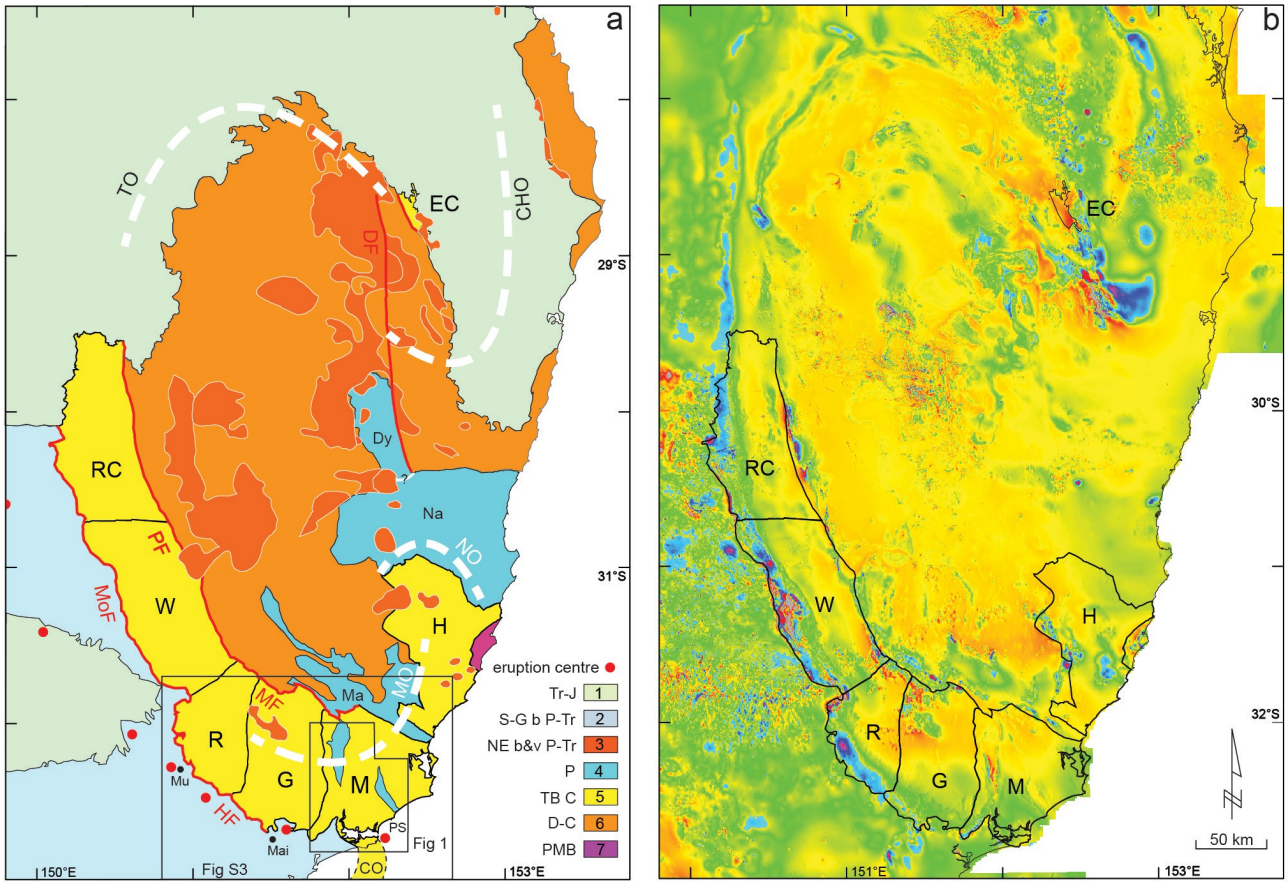

Figure S2. (a) Geological overview map of the SNEO after Raymond et al. (2012) and Phillips et al. (2016). Legend: 1, *T*riassic–Jurassic Great Australian and Clarence-Moreton basins; 2, Permian–Triassic Sydney and Gunnedah basins; 3, Permian–Triassic New England Batholith and volcanics; 4, Permian Nambucca-Dyamberin, Manning, Gloucester and Myall basins; 5, Carboniferous Tamworth Belt (TB) forearc basin; 6, Devonian–Carboniferous accretionary complex; 7, Port Macquarie Block; CHO, Coffs-Harbour Orocline; CO, Currarong Orogen; Dy, Dyamberin Block; EC, Emu Creek Block; G, Gresford Block; H, Hastings Blocks; HF, Hunter Fault; M, Myall blocks; Ma, Manning Basin; Mai, Maitland; MF, Manning Fault; MO, Manning Orocline; MoF, Mooki Fault; Mu, Muswellbrook; Na, Nambucca Block; NO, Nambucca Orocline; PF, Peel Fault; PS, Port Stephens; R, Rouchel Block; RC, Rocky Creek Block; TO, Texas Orocline; W, Werrie Block. Oroclines (white dashed) after Musgrave (2015), Phillips et al. (2016), and Rosenbaum (2018). Offshore Currarong Orogen (CO) after Glen (2013). Dyamberin and Nambucca blocks after Shaanan and Rosenbaum (2018). Eruption centres after Buck (1988), Jenkins et al. (2002), McPhie (1987) and Roberts et al. (1991). (b) Total magnetic intensity (blue = low, red = high) map of the SNEO after Nakamura and Milligan (2015).

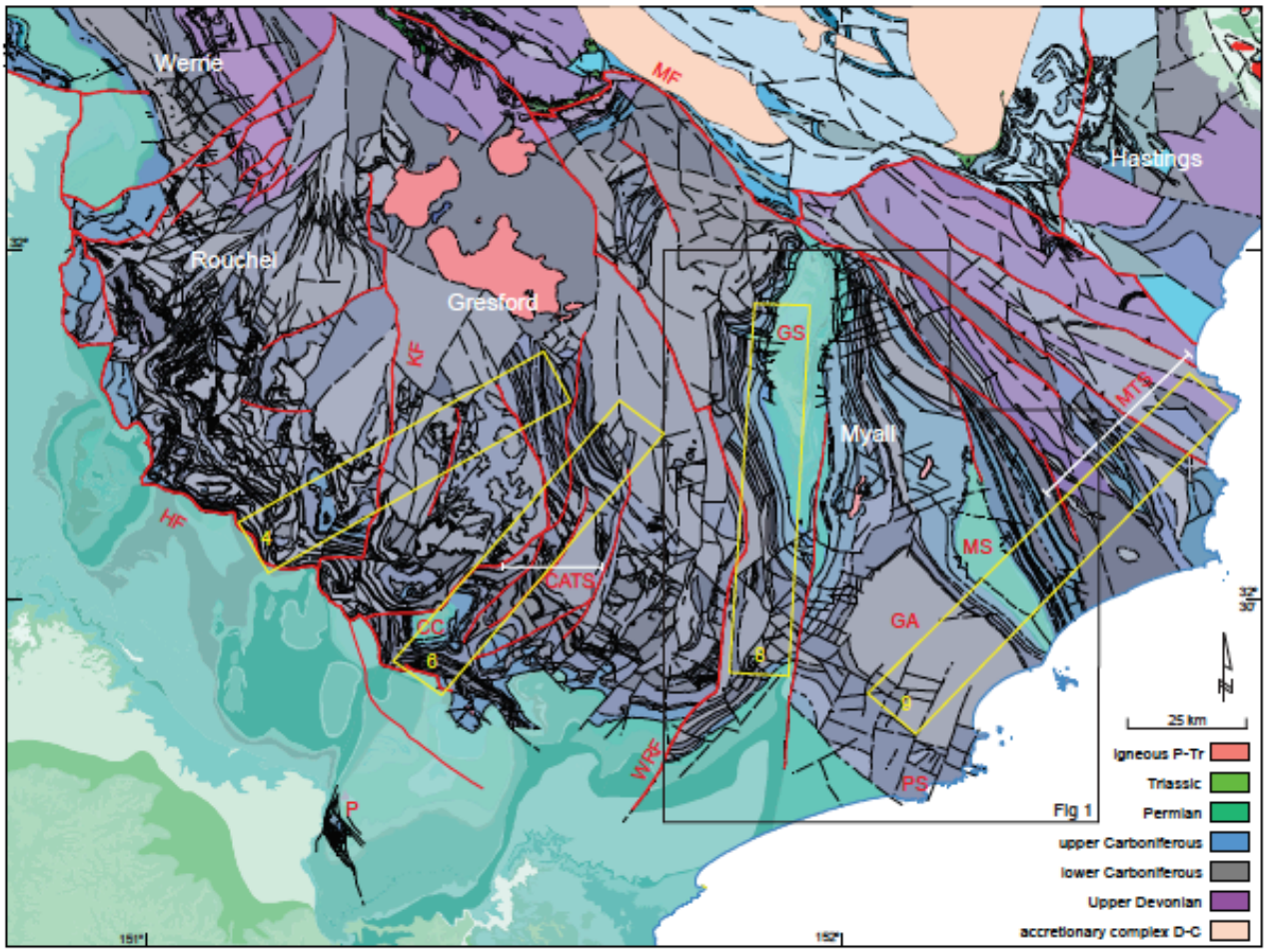

Figure S3. Geological overview map of the southern TB after Phillips et al. (2015, 2016). Yellow rectangles (4, 6, 8, 9) outline sections for stratigraphic ideal columns (Figure 2) after Glen and Roberts (2012, figures 2 and 3). Legend indicates generalised age intervals: CATS, Camyr-Allyn Thrust System; CC, Cranky Corner Basin; GA, Girvan Anticline; GS, Gloucester Syncline; HF, Hunter Fault; KF, Karrakurra Fault; MF, Manning Fault; MS, Myall Syncline; MTS, Myall Thrust System; P, Pokolbin Inliers; PS, Port Stephens; WRF, Williams River Fault.

Figure S4. Zijderveld plots (a–bbb) of progressive thermal and alternating field demagnetisations in geographic coordinates. Circles indicate successive endpoints of magnetisation vector – open circles (connecting red line) projections on vertical east–west or vertical north–south plane, black dots (connecting blue line) on horizontal plane. Numbers denote successive peak temperatures (°C) of heating cycles, or successive peak fields (mT) of alternating field treatments. Red and treatments. Red and blue solid line segments indicate component directions fitted through linear PCA. L1/L2/L3 or L indicate low-temperature overprints of normal polarity and post-folding origin, Ln and Lr low-temperature normal and reverse polarity overprints in Lakes Road Rhyolite Member (aaa) (Table S7) and Lh unique occurrence (site 58) of a high-temperature post-folding overprint comparable in direction to L components. P/P2/N2 indicate pre-folding primary components, with high unblocking temperatures often residing in a mainly hematite carrier, or with intermediate unblocking temperatures for the Nerong Volcanics (Table S2a). P1/N1 likewise indicate incompletely cleaned pseudo-primary components often residing in a mainly magnetite carrier (Table S2b) ('Discussion – Paleomagnetic cleaning bias'). O/Q/T/TT/PT indicate pre-folding overprint components with high unblocking temperatures, or intermediate unblocking temperatures for mainly the Nerong Volcanics (Table S3). Shaded boxes with "ctd" after specimen identifier, indicate partial enlargements. Number between brackets following plot identifier (a–bbb) indicates site (Table S1). Stratigraphic units represented by sets of plots indicated in italics.

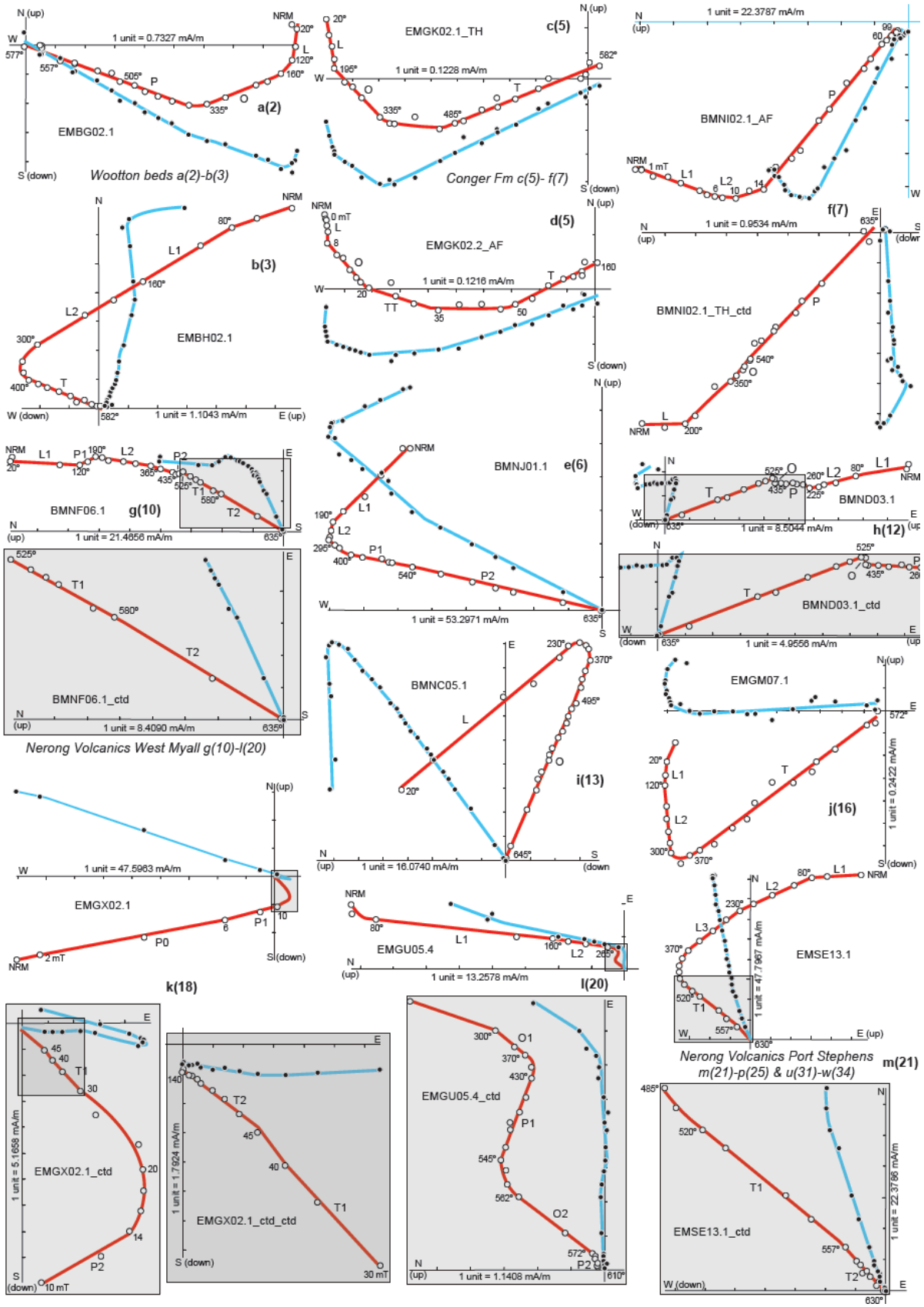
EMBG02.1
1 unit = 0.7327 mA/m
a(2)
Wootton beds a(2)-b(3)
EMBH02.1
b(3)
1 unit = 1.1043 mA/m
EMGK02.1_TH
c(5)
1 unit = 0.1228 mA/m
Conger Fm c(5)- f(7)
EMGK02.2_AF
d(5)
1 unit = 0.1216 mA/m
BMNJ01.1
e(6)
1 unit = 53.2971 mA/m
BMNF06.1
g(10)
1 unit = 21.4856 mA/m
BMNF06.1_ctd
1 unit = 8.4090 mA/m
Nerong Volcanics West Myall g(10)-l(20)
BMNC05.1
i(13)
1 unit = 16.0740 mA/m
EMGX02.1
1 unit = 47.5963 mA/m
k(18)
EMGU05.4
1 unit = 13.2578 mA/m
l(20)
EMGX02.1_ctd
1 unit = 5.1658 mA/m
EMGX02.1_ctd_ctd
1 unit = 1.7924 mA/m
EMGU05.4_ctd
1 unit = 1.1408 mA/m
BMNI02.1_AF
1 unit = 22.3787 mA/m
f(7)
BMNI02.1_TH_ctd
1 unit = 0.9534 mA/m
BMND03.1
h(12)
1 unit = 8.5044 mA/m
BMND03.1_ctd
1 unit = 4.9556 mA/m
EMGM07.1
j(16)
1 unit = 0.2422 mA/m
EMSE13.1
1 unit = 47.7967 mA/m
Nerong Volcanics Port Stephens
m(21)-p(25) & u(31)-w(34)
m(21)
EMSE13.1_ctd
1 unit = 22.3786 mA/m

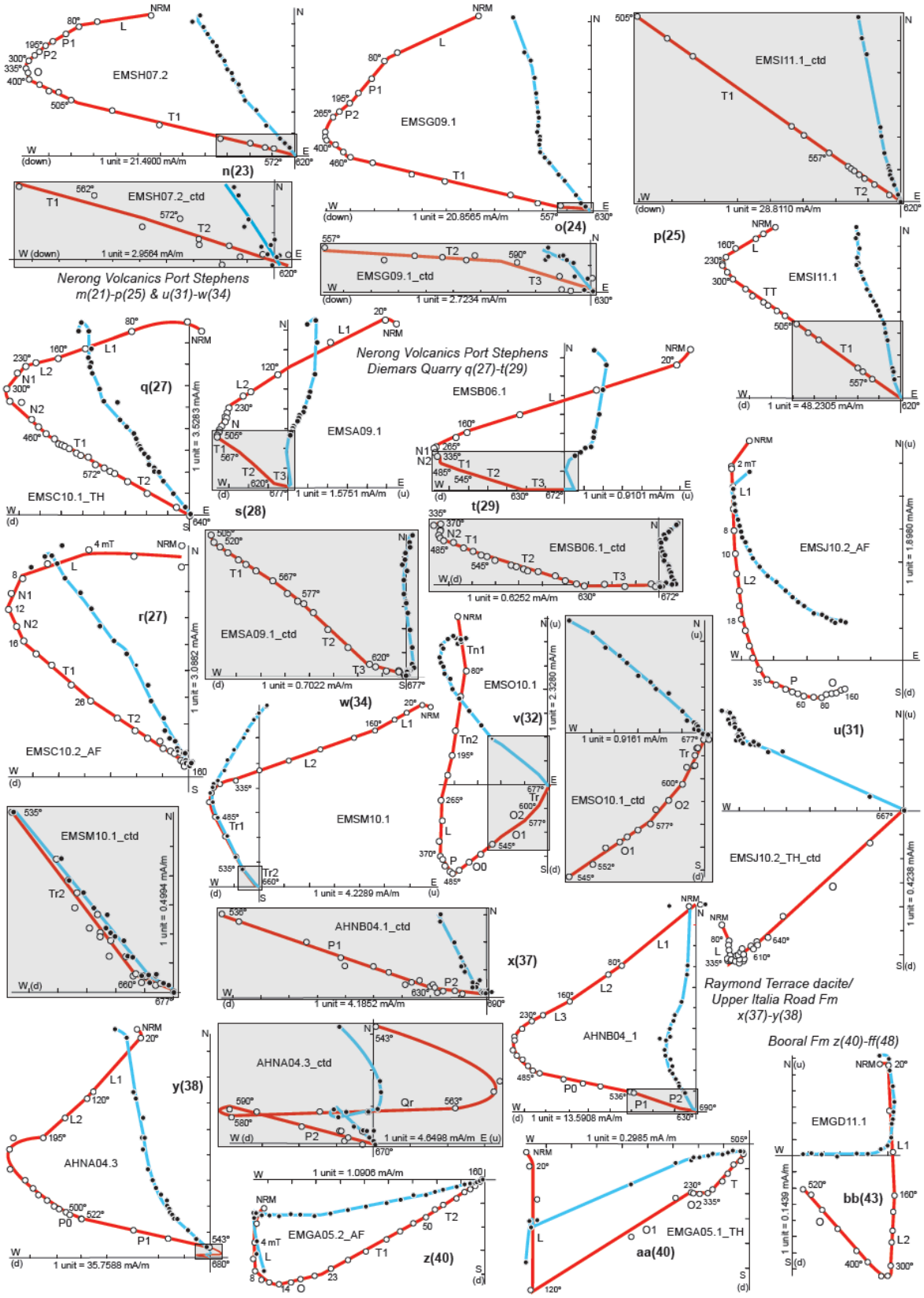
EMSH07.2
n(23)
EMSH07.2_ctd
Nerong Volcanics Port Stephens
m(21)-p(25) & u(31)-w(34)
EMSG09.1
o(24)
EMSG09.1_ctd
EMSI11.1_ctd
p(25)
EMSI11.1
EMSC10.1_TH
q(27)
EMSA09.1
s(28)
EMSA09.1_ctd
Nerong Volcanics Port Stephens
Diemars Quarry q(27)-t(29)
EMSB06.1
t(29)
EMSB06.1_ctd
EMSC10.2_AF
r(27)
EMSM10.1
w(34)
EMSM10.1_ctd
EMSO10.1
v(32)
EMSO10.1_ctd
EMSJ10.2_AF
u(31)
EMSJ10.2_TH_ctd
AHNB04.1_ctd
x(37)
AHNB04_1
Raymond Terrace dacite/
Upper Italia Road Fm
x(37)-y(38)
Booral Fm z(40)-ff(48)
AHNA04.3
y(38)
AHNA04.3_ctd
EMGA05.2_AF
z(40)
EMGA05.1_TH
aa(40)
EMGD11.1
bb(43)

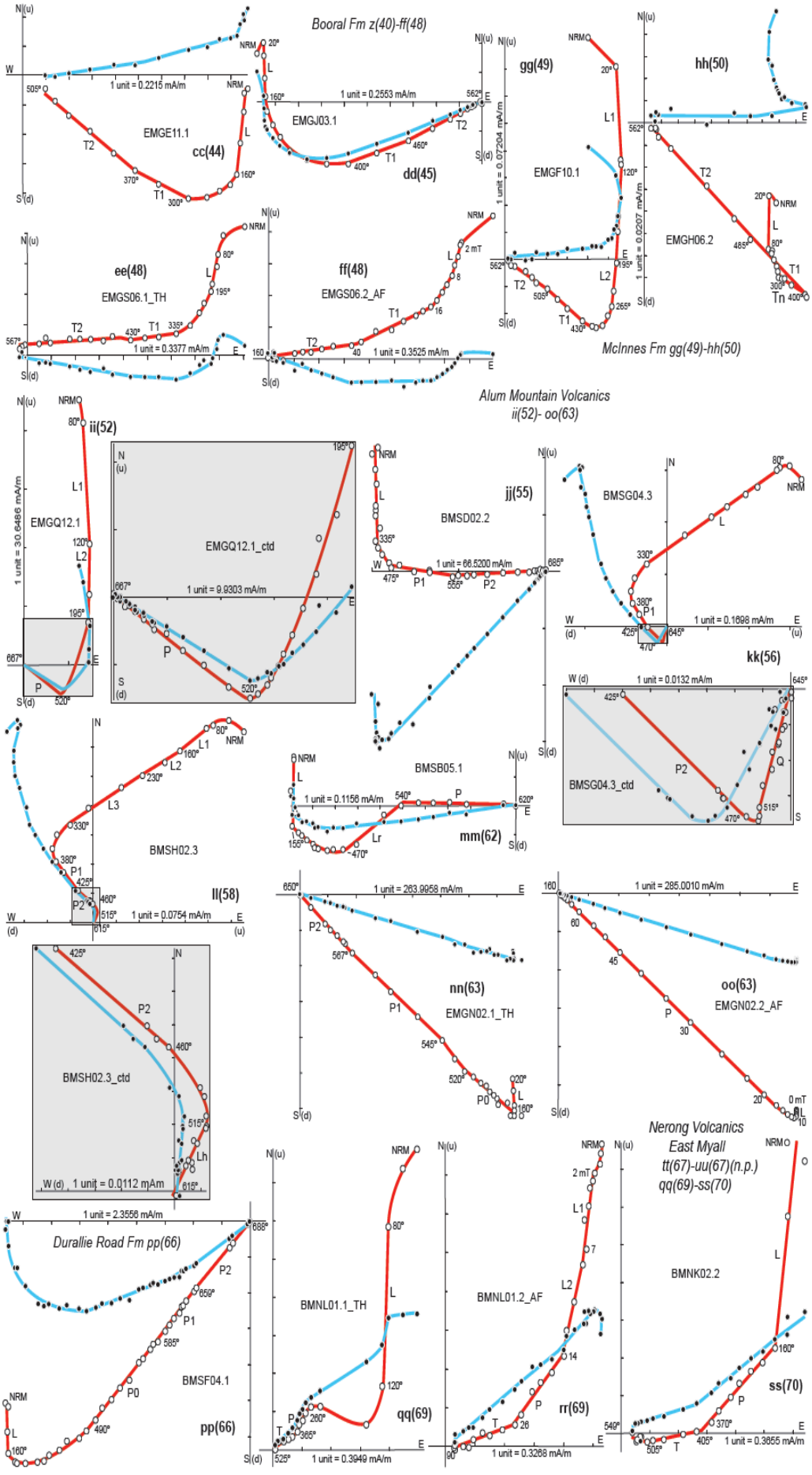
Booral Fm z(40)-ff(48)
cc(44)
EMGE11.1
dd(45)
EMGJ03.1
ee(48)
EMGS06.1_TH
ff(48)
EMGS06.2_AF
gg(49)
EMGF10.1
hh(50)
EMGH06.2
McInnes Fm gg(49)-hh(50)
Alum Mountain Volcanics
ii(52)- oo(63)
ii(52)
EMGQ12.1
EMGQ12.1_ctd
jj(55)
BMSD02.2
kk(56)
BMSG04.3
BMSG04.3_ctd
ll(58)
BMSH02.3
BMSH02.3_ctd
mm(62)
BMSB05.1
nn(63)
EMGN02.1_TH
oo(63)
EMGN02.2_AF
Nerong Volcanics
East Myall
tt(67)-uu(67)(n.p.)
qq(69)-ss(70)
Durallie Road Fm pp(66)
BMSF04.1
pp(66)
BMNL01.1_TH
qq(69)
BMNL01.2_AF
rr(69)
BMNK02.2
ss(70)

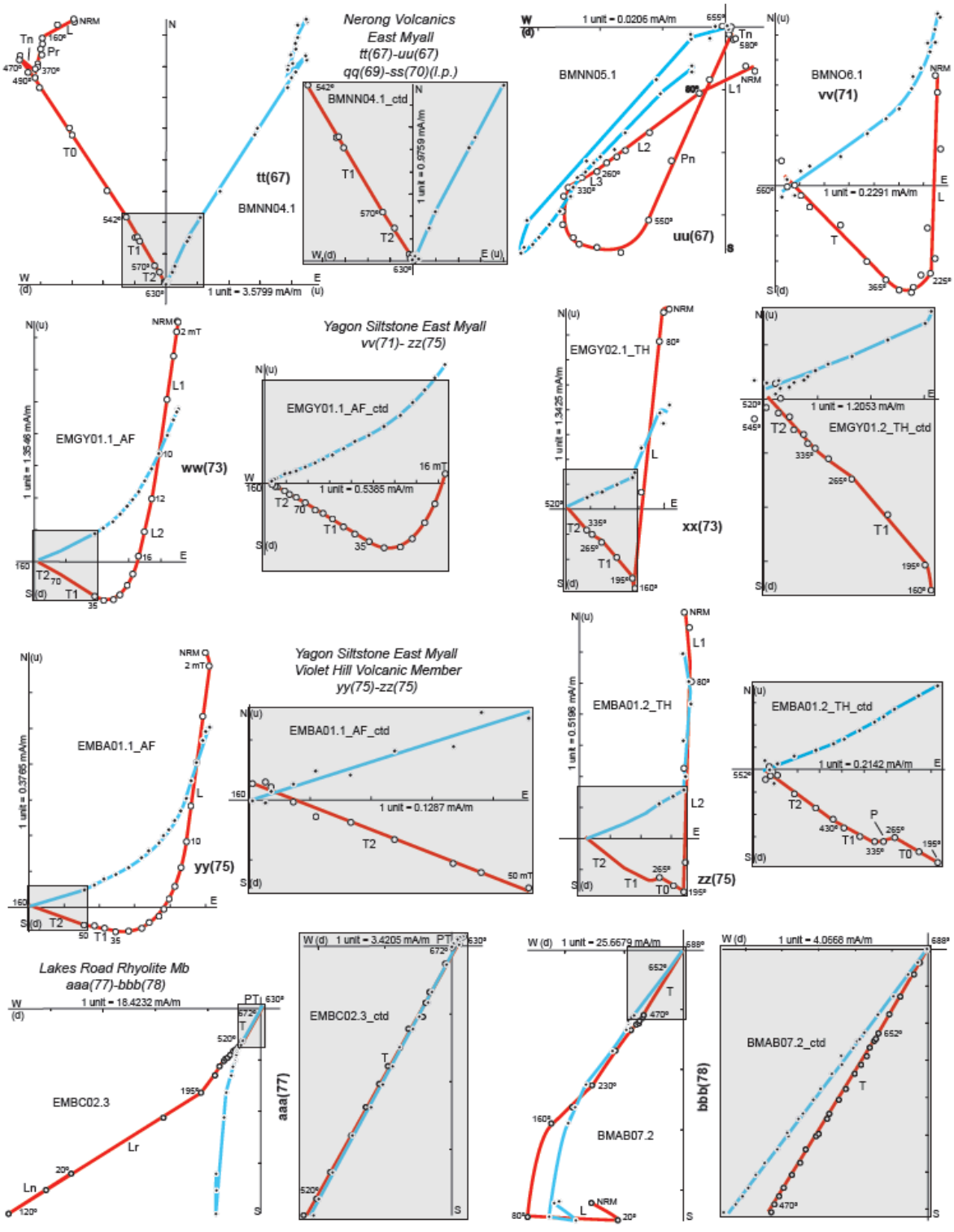
Nerong Volcanics
East Myall
tt(67)-uu(67)
qq(69)-ss(70)(l.p.)
tt(67)
BMNN04.1
BMNN04.1_ctd
BMNN05.1
uu(67)
BMNO6.1
vv(71)
Yagon Siltstone East Myall
vv(71)- zz(75)
EMGY01.1_AF
ww(73)
EMGY01.1_AF_ctd
EMGY02.1_TH
xx(73)
EMGY01.2_TH_ctd
Yagon Siltstone East Myall
Violet Hill Volcanic Member
yy(75)-zz(75)
EMBA01.1_AF
yy(75)
EMBA01.1_AF_ctd
EMBA01.2_TH
zz(75)
EMBA01.2_TH_ctd
Lakes Road Rhyolite Mb
aaa(77)-bbb(78)
EMBC02.3
aaa(77)
EMBC02.3_ctd
BMAB07.2
bbb(78)
BMAB07.2_ctd

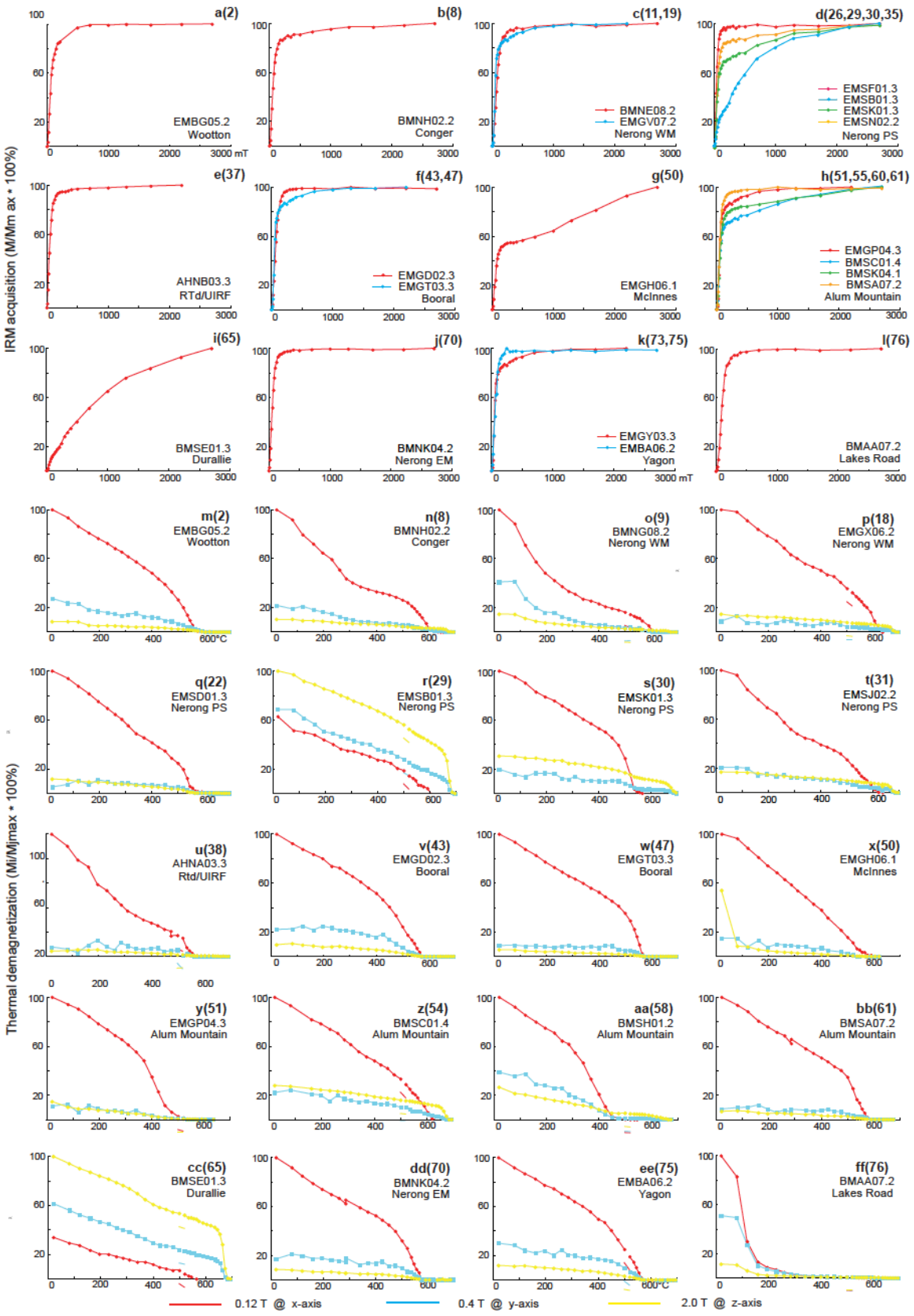

Figure S5. (a–l) Examples of IRM acquisition in constant fields up to 2700 mT. (m–ff) Examples of thermal demagnetisation of three-axis magnetisations (Lowrie, 1990): yellow graph/filled diamonds, hard IRM (2000 mT); blue graph/filled squares, medium IRM (400 mT); red graph/dots, soft IRM (120 mT), magnetisations acquired in order described. Number between parentheses following subfigure label (a–ff) indicates site (Table S1). WM, western Myall Block; EM, eastern Myall Block;PS, Port Stephens region, southwestern Myall Block.

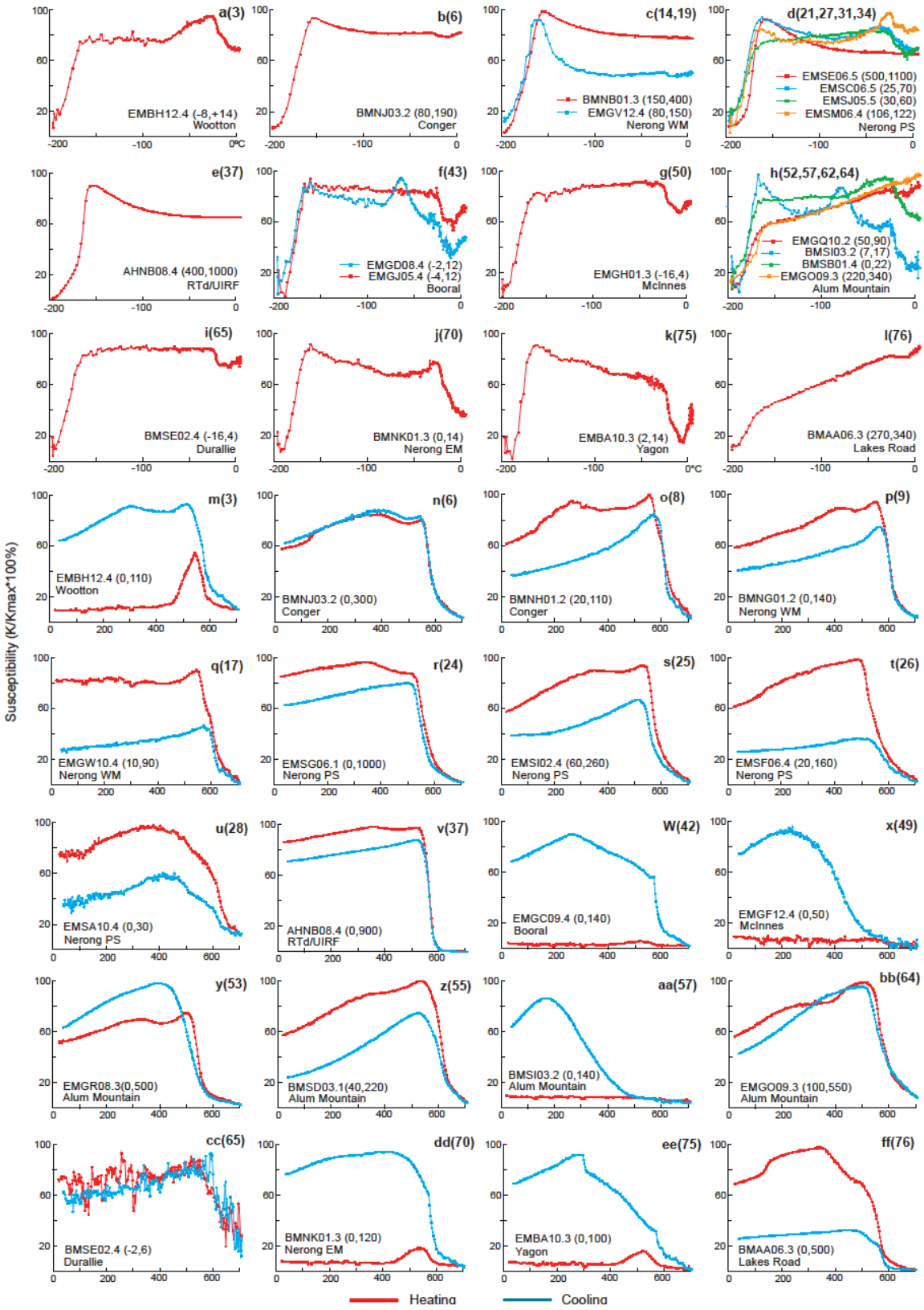

Figure S6. (a–l) Examples of thermomagnetic curves obtained with an AGICO CS-3 cryostat showing susceptibility changes during warming from liquid nitrogen temperatures. (m–ff) Examples of thermomagnetic curves obtained with an AGICO CS-3 furnace showing susceptibility changes during heating (red) and subsequent cooling (blue) carried out in argon gas. Number between parentheses following subfigure label (a–ff) indicates site (Table S1). Numbers between parentheses following specimen identifier indicate susceptibility intensity range in units of 10–6. WM, western Myall Block; EM, eastern Myall Block; PS, Port Stephens region, southwestern Myall Block.

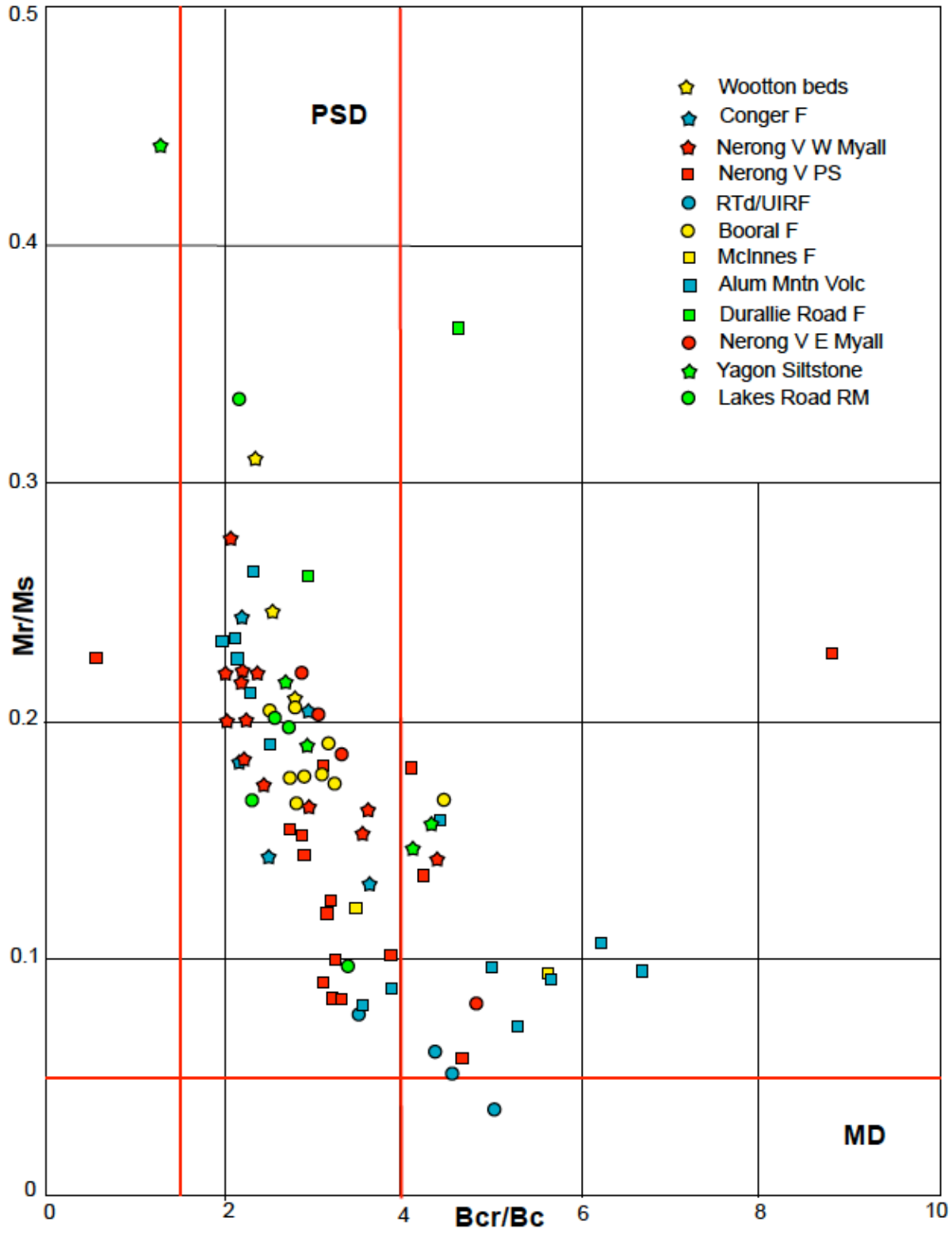

Figure S7. Day *et al.* (1977) plot based on hysteresis parameters Mr, Ms, Bc and backfield parameterBcr. One specimen per site for all sites (N= 80) (Table S1).

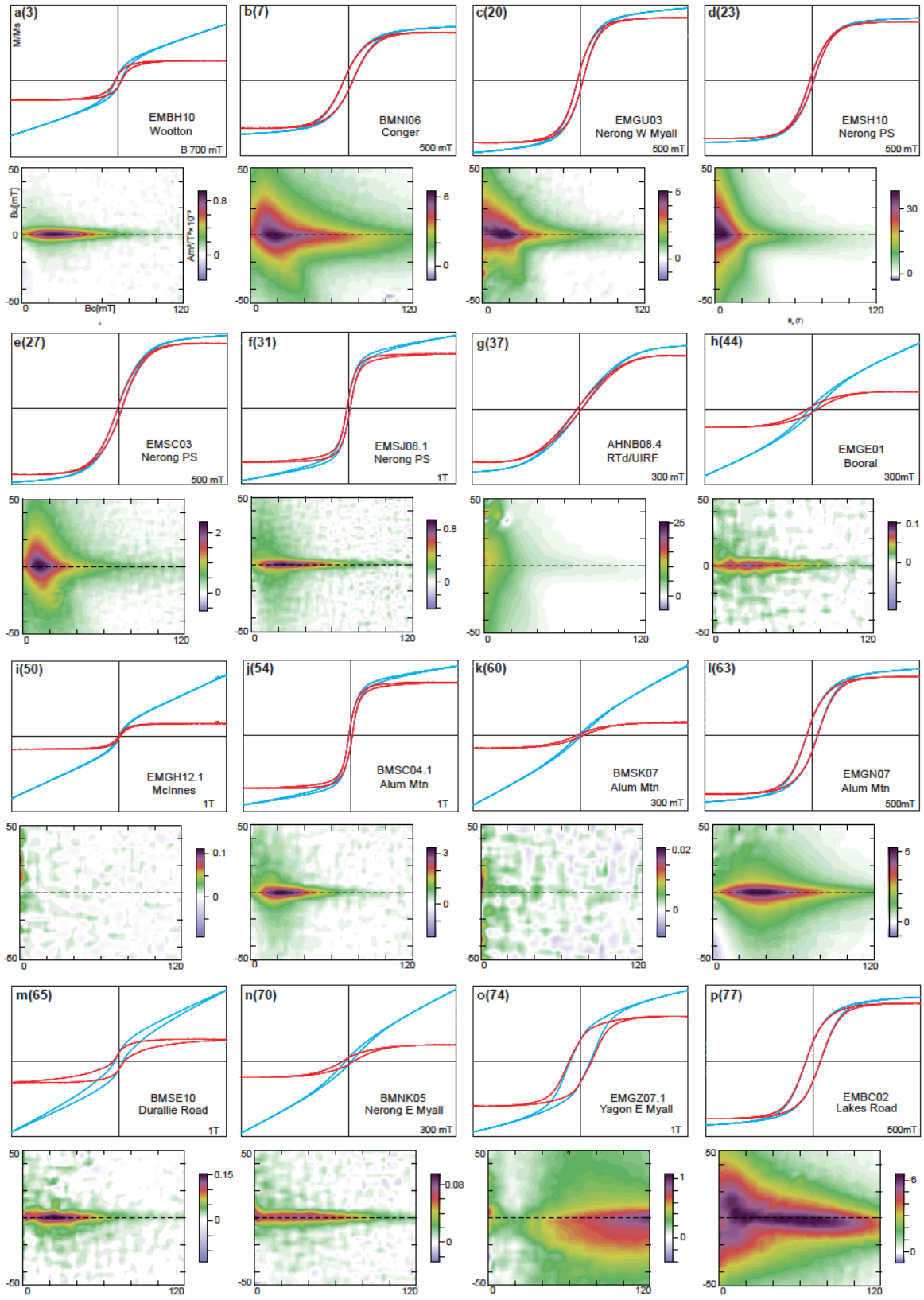

Figure S8. (a–p) Hysteresis curves and corresponding FORC diagrams for representative sites. Hysteresis curves (blue) corrected (red) for paramagnetic content based on saturation at 70% of Bmax. FORC measurements (Roberts et al.,2014) made with averaging times of 200 milliseconds (ms) (b, f, j), 300 ms (a, c–e, g, h, l, p), 400 ms (m) and 600 ms (i, k,n, o) and no repeats, and FORC diagrams processed following Harrison & Feinberg (2008). Number between parentheses following subfigure label (a–p) indicates site (Table S1). W Myall, western Myall Block; E Myall, easternMyall Block; PS, Port Stephens region, southwestern Myall Block.